ATOMIC BEAM SCATTERING STUDIES OF ORDERING AT SURFACES

Klaus Kern and George Comsa

IGV/KFA, P.O. Box 1913
D-5170 Jülich, Federal Republic of Germany

ABSTRACT

The scope of this workshop is to bring the "growth" people and the "surface science" people closer; to make them interact. This contribution tries to parallalize this scope by discussing experimental aspects of the interaction between the substrate surface and the growing film. The focus is on the structure and dynamics of rare gas films growing on close packed metal substrates as investigated by high-resolution He scattering.

The influence of the substrate on the film growth can be easier understood by realizing the crucial role played by the first adsorbed monolayer. Indeed, on the one hand, the properties and in particular the structure of this first layer are decisively influenced by the substrate. On the other hand, the nature of the film growth depends directly on the structure of this first monolayer; e.g. layer-by-layer growth can hardly take place if the structure and the lattice constant of the first monolayer deviate markedly from the equilibrium structure and lattice constant of the bulk material.

The influence of the substrate on the structure and dynamics of the first adlayer proceeds via the strength and lateral corrugation of the holding potential and - in real life - also via the always present defects. The influence of the lateral corrugation of the holding potential on the structure - in particular on the lattice constant and orientation - of the first adsorbed full monolayer will be emphasized. The controversial issue concerning the height of the lateral corrugation is also discussed.

INTRODUCTION

The first monolayer of a film growing on a substrate plays an essential role in heteroepitaxy. Indeed, on the one side of the layer, it has to cope with the surface layer of the substrate, which is made of atoms of a different species, i.e. with different electronic properties, and which in general has a different structure (lattice constant and even symmetry) than the layer would have as a part of its own bulk crystal. As a consequence the properties and in particular the structure of the first adlayer differs into a lesser or larger extent from the properties of the

Kinetics of Ordering and Growth at Surfaces
Edited by M. G. Lagally
Plenum Press, New York, 1990

outermost layer of its own bulk crystal. The nature and magnitude of this difference determine primarily the nature of the film growth on the other side of the adlayer.[1,2] The nature of the atoms on the growing side being the same, even minute structural misfits and the ensuing stress may forbid layer-by-layer epitaxial growth.

Thermal He-scattering proves to be a particularly adequate probe to investigate the various properties of this first monolayer as well as those of the growing film.[3] This is due to features like exclusive sensitivity to the outermost layer, nondestructiveness, high momentum resolution in diffraction, very high energy resolution of energy loss and last but not least outstanding sensitivity for minute impurities and defects. In section 2 the principles and application of He-scattering to adlayer investigation are outlined.

The heteroepitaxial growth is known to be a very complex process. In order to be able to determine important details and to reach clear conclusions concerning main aspects of the process we have chosen to look at simple systems: rare gas films on a close packed metal surface (Xe, Ar, Ne on Pt(111)). The lowest energy surface of the rare gas crystals has the same symmetry as the Pt(111)-surface and the corrugation of the (111) surface of fcc metals is the lowest compared to other orientations. Some of the significant results will be illustrated for the Xe/Pt(111) system; in particular the monolayer statics and dynamics and the multilayer growth.

THERMAL He ATOMS AS A PROBE OF THIN FILM GROWTH AND DYNAMICS

There are several ways of using thermal atom scattering to study the proper- ties of surfaces and adsorbed layers. In this chapter we will outline the different types of surface scattering, emphasizing the features that make He atoms to a particularly appropriate probe of thin film growth and dynamics.

Figure 1 shows schematically a He-atom-surface scattering experiment. A highly monochromatic beam of thermal He-atoms ($\Delta\lambda/\lambda \leq 1\%$) is generated in a high pressure supersonic expansion and collimated to a few tenths of a degree by a series of specially shaped collimators, i.e. so called skimmers. Depending on the source temperature, the wave-length of the He atoms ranges between He 0.3 and 2.0Å; typical fluxes are of the order 10^{19} He atoms/sec·sr. The He atoms scattered from the crystal surface into a well defined solid angle element Ω are detected by an electron impact ionization mass spectrometer. The scattered intensity can be either measured energy integrated or energy resolved. In the latter case, the scattered beam is divided into pulses by a pseudo random (PR) chopper and the times of arrival of He-atoms at the detector are analyzed. Since the initial energy of the He-atoms and the geometry of the experiment are known, the energy transfer during the scattering can be calculated. For experimental details of the spectrometer we refer the reader to Ref. 4.

The attractivity of thermal He-atoms as probe particles for the analysis of the structure and dynamics of surfaces and thin films is inherently associated with the following aspects:

1. The Exclusive Surface Sensitivity of the Method

At large separations the He-atom interacts with the electrons of the surface via induced dipol-dipol interactions. These long range dispersion forces are attractive and decay as z^{-3} with z being the distance between

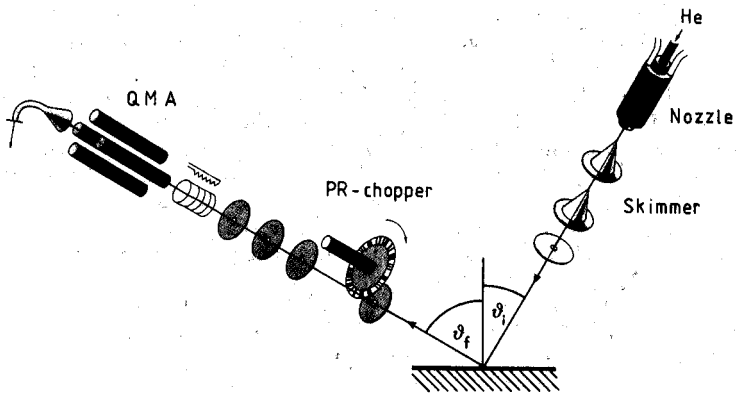

Fig. 1 Schematic arrangement of a He-surface scattering experiment.

He-atom and surface. Upon a closer approach, the electron orbitals of the He-atom overlap with the valence electrons of the surface atoms causing a strong repulsion, which is usually assumed to be proportional to the electron density $\rho(\underline{r})$ of the solid surface. A reasonable Ansatz for the atom surface potential thus writes:[5]

$$V(x,y,z) = V_o \exp[-\kappa(z-\xi(x,y))] - \frac{C_3}{(z+z_o)^3} , \qquad (1)$$

with the constants V_o and z_o, the so called "softness parameter" κ, and the van der Waals-coefficient C_3. In this simple model, the periodic part of the potential given by the modulation $\xi(x,y)$ of the electron density $\rho(\underline{r})$ and reflecting the discrete symmetry of the surface in the x-y plane, only appears in the repulsive part of the interaction potential. The classical turning point of the He-atom is a few angstroms above the ion cores of the surface, i.e. the He-atoms do not penetrate into the selvedge. Accordingly the information sampled by the scattered He-atom is exclusively determined by the outermost surface layer.

2. The Complete Nondestructiveness of the Method

He being a noble gas at very low thermal energies ($\sim$ 10-200 meV), He-atom scattering is a completely nondestructive surface probe. This property is of particular importance in the investigation of weakly bound and sensitive adlayer structures, like physisorbed films with binding energies less than $\sim$300 meV.[3]

3. Energy - Wavelength Matching

The de Broglie wavelength of the thermal He-atoms generated in the super-sonic expansion is comparable to the interatomic spacing and the translational energy is close to the energy of collective surface excitations (e.g. surface phonons). This favorable energy-wavelength matching allows the spectroscopy of static as well as dynamic properties of solid surfaces and thin films.

The matching of the He-atom wavelength with typical interatomic distances of surfaces gives rise to interference effects in the scattering which can be detected by scanning the scattering angle or the wavelength. In such a diffraction experiment no energy analysis is usually done, i.e. the differential cross section $d\sigma/d\Omega$ is measured.[6] In some special experiments the energy analysis of the scattered He-atoms may be used to separate the true elastic scattering.[7] For diffraction from a periodic two dimensional array atoms the structure factor does not depend on the momentum transfer perpendicular to the surface (we are dealing here with diffraction rods!) and the differential cross-section denotes

$$\frac{d\sigma}{d\Omega} \propto S(Q'', \hbar\omega = 0) = \sum_m \delta\ (Q''-G_m'') \ . \qquad (2)$$

The terms $Q'' = (Q_x, Q_y)$ and $G_m'' = (G_{mx}, G_{my})$ are the momentum exchange vector and the reciprocal lattice vector in the surface plane of the two-dimensional structure, respectively. Thus, the Laue-condition for diffraction from a 2D-lattice reads

$$Q'' = G_m'' \ . \qquad (3)$$

The momentum-resolution of the He-diffractometer is determined by the angular opening of the He-beam and of the detector and by the monochromaticity of the He-wave. The instrument used in the authors laboratory, designed to measure also dynamical surface properties in the same experiment (which is achieved at the expense of very high diffraction capabilities) has a momentum resolution of ~ 0.01 Å^{-1}.

In Fig. 2 we show as an example a He-diffraction scan from a complete Xe-monolayer adsorbed on Pt(111) ($\theta_{Xe} \approx 0.42$ Xe-atoms per Pt substrate atoms); a well behaved diffraction pattern with sharp Bragg-peaks is observed. This diffraction scan has been measured in a fixed scattering geometry $\theta_f+\theta_i = 90°$ by rotating the Pt-crystal around an axis perpendicular to the scattering plane; the angle on the abscissae scales to a momentum transfer scale by the relation $Q'' = 5.723\ (\sin\theta_f - \cos\theta_f)$. The diffraction pattern characterizes a hexagonal densely packed 2D-Xe crystalline solid with a nearest neighbor distance of 4.33Å. In the inset of Fig. 2 the orientational structure (with respect to the Pt-substrate) of the Xe-monolayer is characterized in an azimuthal diffraction profile, which is obtain by rotating the Pt-crystal around its surface normal at a fixed polar angle corresponding to a Bragg-position. The symmetric peak-doublet centered along the $\bar{\Gamma}\ \bar{K}_{Pt}$ direction of the substrate surface characterizes a Novaco-McTague phase rotated ± 3.3° degrees off the natural R 30° orientation of submonolayer Xe-films (see Chapter 3.2).

The energy of thermal He atoms is comparable with the energy of most atomic motions of surfaces and overlayers.[8] Thus, in a scattering experiment the He-atom may exchange an appreciable part of its energy with the surface. This energy can be measured in time-of-flight experiments with a resolution of $\sim$0.3 meV. The range of energy transfer that can be covered by thermal He atoms is limited at the low end by the present maximum resolution of $\sim$ 0.3 meV and at the upper end by the nature of the scattering mechanism. The interaction time of thermal He atoms with the surface being of the order of 10^{-13} sec, the upper limit for observable collective excitations is about 40 meV.

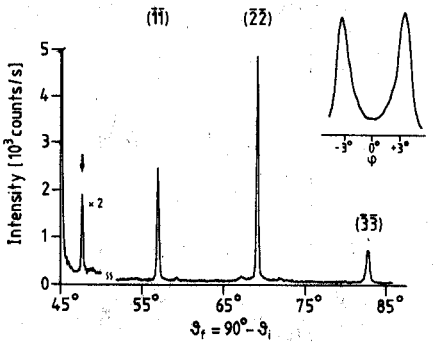

Fig. 2 Polar and azimuthal (inset) He-diffraction scan of a complete Xe monolayer on Pt(111); He wavelength λ_i = 1.098 Å, surface temperature 25 K. The polar scan is taken along the Γ M_{Xe} azimuth.

The kinematics of inelastic He-scattering is governed by conservation of momentum and energy. Because of the loss of vertical translational invariance at the surface, only the momentum parallel to the surface is conserved in the scattering process,

$$K_f = K_i + Q'' + G''_m \tag{4}$$

$$\hbar\omega = \hbar^2 k_f^2/2m - \hbar^2 k_i^2/2m \ , \tag{5}$$

where Q" and $\hbar\omega$ are the phonon momentum and energy respectively, m is the mass of the He-atom, k_i (k_f) and K_i (K_f) are the wave vectors and their components parallel to the surface of incident (scattered) He-atoms, and G''_m is a reciprocal-lattice vector. Depending on the sign of ω, a phonon is annihilated (ω>0) or created (ω<0) during the scattering process. Thus, by inelastic He-atom scattering from surfaces we can measure the dispersion relations of the collective excitations point by point by observing where in the (Q",$\hbar\omega$) space the He-atoms undergo one-phonon annihilation or one-phonon creation events.[8] Formally, what we are measuring in this experiment is the double differential cross section

$$\frac{d^2\sigma}{d\Omega_f dE_f} \propto \sum_{\vec{Q}'',j} |\vec{e}\,(Q'',j) < \Psi_G^{f*} |\nabla V(Q'',z)\, |\Psi_G^{i} > |^2 \times |n^{\pm}| \times$$

$$\delta\,(\vec{K}_f - \vec{K}_i - \vec{Q}'') \times \delta\,(E_f - E_i - \hbar\omega\,(Q'',j)) \ , \tag{6}$$

which describes the exchange of a single phonon of wavevector Q", frequency ω(Q",j) and polarization e(Q",j). The Bose factor for annihilation (-) or creation (+) of a phonon, respectively, i.e., the phonon occupation number, is denoted by $n^{\pm}$.

Figure 3 shows a series of typical He-energy loss spectra which have been measured under identical scattering conditions from Xe-films on Pt(111) 1,2,3, and 25 monolayers (ML) thick. By varying the scattering conditions complete phonon dispersion curves for each film can be plotted (see Ref. 9).

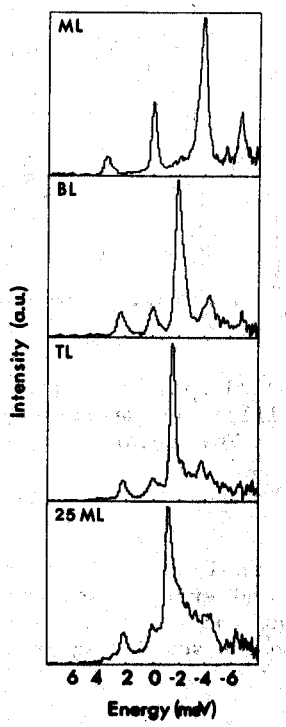

Fig. 3 He energy loss spectra measured in the $\bar{\Gamma}\,\bar{M}_{Xe}$-azimuths of Xe-films on Pt(111) 1, 2, 3, and 25 monolayers thick. All spectra are taken under identical scattering conditions, i.e., primary beam energy 18.4 meV and incident angle $\theta_i = 42°C$.

These dispersion plots reveal a layer-by-layer evolution of the dynamical film properties with thickness. The monolayer film is characterized by a dispersionless Einstein-oscillator. The vibrational modes of multilayer films show dispersion across the Brillouine-zone, the amount of dispersion increases with the film thickness. Eventually, 25 ML-films exhibit a well developed Rayleigh-wave, characteristic for a semi-infinite crystal.

There are two significant features evidenced by the energy loss spectra which are particularly useful in the investigation of film growth. Due to the high resolution, the energy losses (gains) of 1,2 and 3ML films, measured under identical scattering conditions, can be clearly discriminated. This allows the straightforward determination of the completion of the first and of the second monolayers within a few percent. This kind of information is very valuable also in the study of the thermodynamics of physisorbed films.[10] The other feature is the diffuse elastic peak ($\Delta E = 0$), its intensity being known to be a sensitive measure for the presence of surface defects. In Fig. 3 the diffuse elastic intensity decreases with film thickness, which is a direct proof of the layer-by-layer growth of the film.

The energy transfer between a He-atom and a surface is not restricted to collective excitations such as phonons. The He-atom can exchange energy with individual atoms diffusing on the surface. Diffusive motions of adatoms are associated with a continuum of low energy excitations and the interaction of He-atoms with this continuum gives rise to a broadening δE of the elastic peak. For low energy He-scattering from a two-dimensional fluid adlayer, Levi et al.[11] have shown that the width of the "quasielastic" peak is related to the diffusion coefficient D via $\sigma E = 2\hbar DQ^2$. Frenken et al. have recently used this technique to study the self diffusion of Pb adatoms on the Pb(110) surface.[11]

Another remarkable way to use He scattering for the study of adsorbed layers is based on the large ($\sim$ 100 Å^2) total cross-section $\sum$ for diffuse He scattering of isolated adsorbates.[12] This large cross-section is attributed to the long-range attractive interaction between the adatom and the incident He atom, which causes the He atoms to be scattered out of the coherent beams. The remarkable size of the cross-section, 4-6 times the geometrical size, A, of the adsorbate allows the extraction of important information concerning the lateral distribution of adsorbates, mutual interactions between adsorbates, dilute-condensed phase transitions in 2D, adatom mobilites, etc., simply by monitoring the attenuation of one of the coherently scattered beams.[12] This technique also allows the detection of impurities (including hydrogen!) in the permill range, a level hardly attainable with almost all other methods.

The possibility to investigate the lateral distribution of adsorbates, in particular the dilute-condensed phase transition in 2D, is based upon the large difference between the cross-section for diffuse scattering, $\sum$, and the geometrical size, A, of the adsorbates. The degree of overlap of the cross-sections $\sum$ at a certain adsorbate coverage, θ, which determines the He-reflectivity, depends on the nature of the lateral distribution of the adsorbate. For instance, as long as the adsorbates form a lattice gas, the He-reflectivity depends on θ as

$$I/I_o = (1-\theta)^{\Sigma n_s} , \qquad (7)$$

with I_o and I the intensities of the specular beam scattered from the clean and the adsorbate covered surface, respectively, and n_s the density of adsorption sites. At low coverages Eq. (7) becomes

$$I/I_o \simeq 1 - \Sigma\, n_s\, \theta . \qquad (7')$$

On the other hand, when islanding starts, i.e., at the 2D gas → 2D solid + 2D gas transition, the He-reflectivity is determined by the much smaller geometrical size, A, of the adatoms in the 2D condensed phase:

$$I/I_c \simeq 1 - An_s\,(\theta-\theta_c) , \qquad (8)$$

with I_c being the specular intensity at the critical coverage θ^c, where condensation sets in. A comparison of eqs. (7) and (8) shows that the slope of the specular He-intensity I versus coverage θ is expected to change dramatically in the ratio $\sum/A$ ($\simeq$ 4-6) when condensation sets in. This is illustrated in Fig. 4 for a Pt(111) surface at 54 K exposed to Kr at P_{Kr} 2.1×10^{-9} mbar.

The sudden slope change in Fig. 4 obviously marks directly the onset of islanding. The critical coverage θ_c corresponds to the 2D vapor pressure of Kr on Pt(111) at 54 K. From measurements of θ_c at different temperatures, the 2D latent heat of vaporization is obtained under the

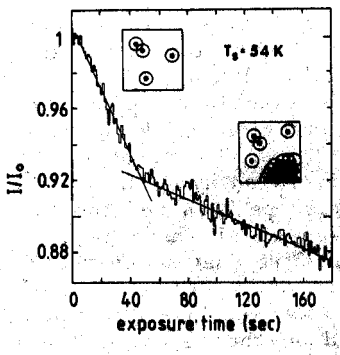

Fig. 4 Attenuation of the specularly reflected He-beam from Pt(111) upon exposure to Kr (P_{Kr} = 2.1 x 10^{-9} mbar) at T_s = 54 K.

assumption that the 2D gas is nearly perfect.[13] In Table I the 2D latent heats of vaporization obtained in this way for Xe, Kr, and Ar on Pt(111) are listed.[3] They represent actually the lateral energy between the adlayer atoms.[12,14]

In addition, at lower temperatures where $\theta_c \to 0$ Eq. (8) can be used in a straightforward manner to determine the sticking probability. Figure 5 shows the same type of measurement as Fig. 4 but at 25 K. The linear drop of the specular intensity with exposure, indicates a coverage-independent sticking coefficient. A simple kinetic calculation gives a value $s_o \approx 0.7$. Only close to completion of the first monolayer (determined by phonon-spectroscopy to be at an exposure of 7.2 x 10^{-6} mbar . sec) the curve deviates from Eq. (8) and eventually levels off.

MONOLAYER FILMS AND STATICS OF COMPETING INTERACTIONS

The properties of monolayer films on solid surfaces, i.e. quasi two dimensional (2D) systems, are quite often different from those of the three dimensional (3D) bulk material. For instance, a one monolayer solid Xe phase melts at a substantial lower temperature than the bulk Xe-solid; on the basal plane of graphite the monolayer Xe-film has a 2D gas-liquid-incommentsurate solid triple point at $T_t^{2D} = 0.61\ T_t^{3D}$.[15] Upon increasing thickness, the film properties gradually approach three dimensional behavior.

Table 1
Lateral Interaction Energies for Rare Gases Adsorbed on Pt(111)

	Xe	Kr	Ar
e_1(meV)	43	26	12

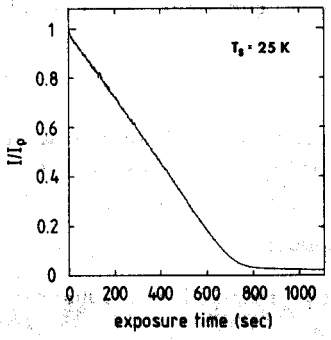

Fig. 5 Same as Fig. 4 but at a surface temperature of T_s = 25 K and a Kr pressure $P_{Kr} = 8.4 \times 10^{-9}$ mbar.

What makes the difference between a monolayer film and a film, say 25 monolayers thick, which shows almost bulk behavior? First, the average atom in a bulk film has twelve nearest neighbors (when condensing in a fcc lattice) while an atom in a monolayer film has only six of the same kind. Thus, thermal fluctuations are more important in monolayer than in bulk films. Second, real adsorbent surfaces are structured, providing a periodic potential relief which interferes with the lattice structure of the overlayer, inducing modulations in the latter.[16] The properties of the first monolayer are certainly influenced most dramatically by the substrate surface. The thicker the grown film the smaller the direct influence of the substrate on the properties of the remote film layers. However, we have to take into account that the film growth depends directly on the structure of this first monolayer. We will thus first discuss the static interaction of substrate and adlayer in the monolayer regime.

1. Substrate Corrugation and Commensurability

Atoms adsorbed on a periodic substrate can form ordered structures. These structures may be either in or out of registry with the structure of the substrate. It is convenient to describe this ordering by relating the Bravais lattice of the adlayer to that of the substrate surface. Park and Madden[17] have proposed a simple vectorial criterion to classify the structures. Let a_1 and a_2 be the basis vectors of the adsorbate and b_1 and b_2 those of the substrate surface; these can be related by

$$\begin{bmatrix} \vec{a}_1 \\ \vec{a}_2 \end{bmatrix} = F \begin{bmatrix} \vec{b}_1 \\ \vec{b}_2 \end{bmatrix} \tag{9}$$

with the matrix

$$F = \begin{bmatrix} F_{11} & F_{12} \\ F_{21} & F_{22} \end{bmatrix} ; \tag{10}$$

$a_1 \times a_2$ and $b_1 \times b_2$ are the unit cell areas of the adlayer and substrate surface, respectively; det F is the ratio of the two areas. The relation

between the two ordered structures is classified by means of this quantity as follows:

i) det F = integer

the structure of the adlayer has the same symmetry class as that of the substrate and is in registry with the latter; the adlayer is termed commensurate.

ii) det F = irrational number

the adlayer is out of registry with the substrate; the adlayer is termed incommensurate.

iii) det F = rational number

the adlayer is again in registry with the substrate. However, whereas in i) all adlayer atoms are located in equivalent high-symmetry adsorption sites, here only a fraction of adatoms is located in equivalent sites; the adlayer is termed high-order commensurate.

In Fig. 6, we show a simple one-dimensional model illustrating this classification. The periodicity of the substrate surface is represented by a sinusoidal potential of period b and the adlayer by a chain of atoms with nearest neighbor distance a.

Assuming that the structural mismatch between adlayer and substrate is not too large (≤10-15%), the nature of the adlayer ordering on the substrate is determined by the relative interaction strength e_1/V_c which is the ratio of e_1, the lateral adatom interaction in the layer, to V_c, the modulation of the adsorbate-substrate potential parallel to the surface. When the diffusional barrier Vc is large compared to the lateral attraction, commensurate structures will be formed. On the other hand, when the lateral adatom interactions dominates, incommensurate structures will be favored. Only when the competing interactions are of comparable magnitude, may both registry and out of registry structures be stabilized by the complex interplay of these interactions.

Before discussing some examples of structural monolayer phases and their mutual transitions, it seems useful to comment shortly on the substrate corrugation V_c. Remember: V_c corresponds to the modulation along the surface of the bottom of the adsorbate-surface potential well. Its magnitude has been often underestimated because it has been correlated with the corrugation felt by a thermal He atom when scattering at the surface. With respect to the corrugated felt by an adsorbed Xe atom migrating along the surface there are two fundamental differences: the scattering atom feels the corrugation of the repulsive potential and not that of the bottom of the attractive well and the polarizability of He is about 20 times smaller than that of Xe.

It has been shown by Steele,[18] that the physisorption potential of rare gas atoms on a crystal surface is represented, in a good approximation, by a Fourier expansion in the reciprocal lattice vectors G of the substrate surface

$$V(r,z) = V_o(z) + V_{mod}(r) = V_o(z) + \sum_G V_G(z) \exp(iGr) , \qquad (11)$$

evidencing nicely the lateral modulation of the adsorption energy. Here z (> 0) is the distance of the adatom perpendicular to the surface and r the coordinate parallel to the surface. $V_o(z)$ is the mean potential

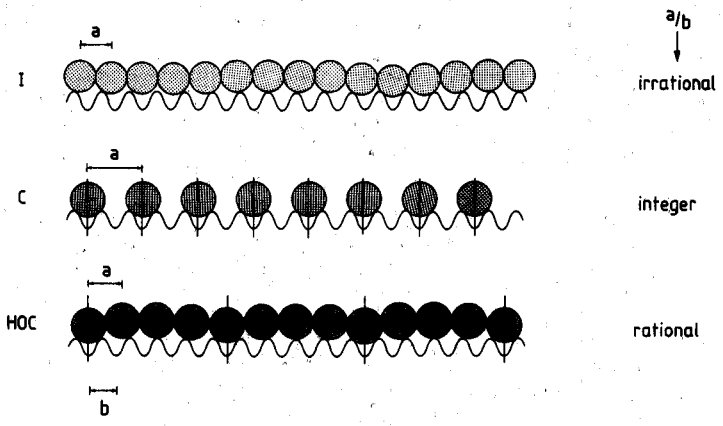

Fig. 6 One-dimensional model for adsorbed monolayers. The substrate is represented by a sinusoidal potential of period b and the adlayer by a chain of atoms with lattice constant a. C-commensurate, HOC-high order commensurate, and I-incommensurate.

energy of an adatom at a distance z, V_G the principal Fourier amplitude. At low temperatures $V_o(z)$ can be replaced by its harmonic approximation:

$$V_o(z) \simeq V_o + V_o'' (z-z_o)^2 \quad . \tag{12}$$

Owing to the rapid convergence of the Fourier series, the second term is usually already one order of magnitude smaller than the first order term, and for the basal plane of graphite Gr(0001) and the fcc(111) surface we obtain

$$\vec{V}(r) = V_o(z) + V_G \{\cos(2\pi s_1) + \cos(2\pi s_2) + \cos 2\pi(s_1+s_2)\} \tag{13}$$

respectively. Here s_1 and s_2 are the dimensionless coordinates of the atoms in the substrate surface unit cell (see Fig. 7).

If we assume a 12-6 Lennard-Jones pair potential to represent the interaction between various atoms of the adsorbate/substrate system, the corrugation in the unit cell of a particular surface is entirely determined by the ratio σ/a and by the magnitude of the binding energy V_o, with σ being the Lennard-Jones diameter of the adatom and a being the nearest neighbor distance in the substrate surface. In this model, the energy difference between adsorption of a Xe-atom in a hollow and in a bridge position, V_{H-B}, amounts to $\sim 0.02\ V_o$ for the graphite (0001) surface and to $\sim 0.01\ V_o$ for the (111) surfaces of Pd, Pt and Ag (similar atomic radii).[18] It is this energy difference between desorption in a hollow site and in a bridge site which represents the corrugation of the potential which determines the activation barrier for the diffusive motion of adatoms and thus ultimately also whether, at a given natural misfit between adlayer and substrate, commensurate structures appear. Taking the actual binding energies for Xe-adsorption on these surfaces,[10,14] the Xe-corrugation is calculated to $\sim$ 3 meV (Gr), $\sim$ 3 meV (Pd, Pt) and $\sim$ 2 meV (Ag).

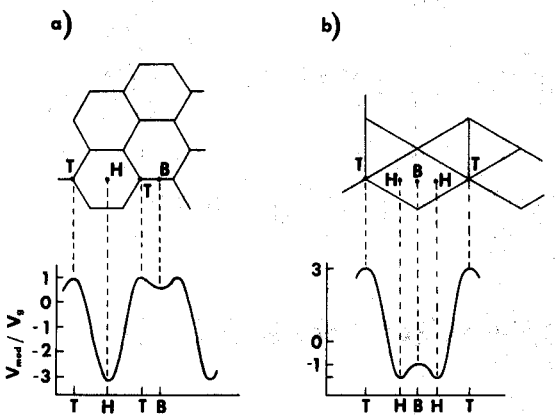

Fig. 7 The variation of the well depth of the rare gas/graphite (0001) (a) and rare gas/Pt (111) (b) potential in the plane parallel to the substrate surface, in the framework of a simple Lennard-Jones model (see text).

The two-body Lennard-Jones potential is only a crude approximation of the interaction between a rare gas atom and a solid surface. While for the rare gas-graphite interaction the inclusion of many body terms, in particular three body forces, significantly improves the physisorption potentials, this approach seems to be insufficient in the case of metal surfaces. Drakova et al.[19] demonstrated recently in a self consistent Hartree-Fock calculation, that the corrugation of the rare gas-transition metal surface potential is substantially enhanced by the hybridization between occupied rare gas orbitals and empty metal d-orbitals. For the interaction of a Ne-atom with the (110) surface of Cu, Ag and Pd, these authors calculated the corrugation of the short bridge site, V_{H-SB} to increase from 0.04 V_o (Cu) over 0.08V_o (Ag) to 0.27 V_o (Pd). Based on the Pd(110) value we can estimate the bridge corrugation V_{H-B} of the (111) surfaces of Pd and Pt to about 0.07-0.08 Vo and that of Ag to about 0.02 Vo" These large values are consistent with the semiempirical Xe-Pd potential, recently developed by Girard and Girardet[20] in order to explain the experimentally observed face specificity of the binding energy and of the induced dipole moment. For Pd(111) these authors evaluated $V_{H-B} \simeq V_o$, and for the Pd(110) surface they calculated $V_{H-SB} \simeq 0.35\ V_o$.

A similar trend also holds for the graphite-rare gas interactions; including anisotropic interactions between the adatom and each carbon atom Vidali and Cole[21] calculate, for example, a corrugation V_{H-B} 0.04 V_o $\simeq$ - 6 meV for the Xe-atom, which is twice the original value given by Steele. This corrugation seems to be fairly consistent with various experimental results.

The large rare gas-d-metal corrugation has been confirmed recently in experiments and in molecular dynamics studies of Xe adsorption on Pt(111). From the Xe-coverage dependence of the isosteric heat of adsorption, Kern et al.[22] determined the corrugation of the Xe/Pt(111) potential to $\sim$ 30 meV, i.e. about 10% of the binding energy (V_0 = 277 meV in the limit of zero coverage[10]). A somewhat lower value of $\sim$ 10 meV was

needed in a molecular dynamics simulation by Black and Janzen[23] in order to stabilize the commensurate $\sqrt{3}$ Xe-phase which has been observed experimentally (see below). Note, that these relatively larger values are compatible with values of diffusion barriers determined in direct experiments on other close packed surfaces as for instance, for Xe on W(110) yielding 47 meV[24].

2. Monolayer Phases of Xe on Pt(111)

As already stated, when the lateral adatom interaction and the substrate corrugation are comparable, the adsorbed monolayer may form various ordered structures, commensurate as well as incommensurate phases allowing the investigation of the corresponding CI-transition as a function of coverage or temperature. In view of the lateral interaction energy e_1 = 43 meV of Xe on Pt(111) and the similar value of the corrugation $V_c \approx 30$ meV, this adsorption system should be a model system to test the ordering phenomena in two dimensional systems with competing interactions. The Xe-Xe and Xe-Pt interactions favor Xe adsorption in the three fold hollow sites of the Pt(111) surface. Below coverages of $\theta_{Xe} \approx$ 0.33 (Xe adatoms per Pt-substrate atoms) and in the temperature range 60-99 K the xenon condenses in a ($\sqrt{3}$ x $\sqrt{3}$)R30° commensurate solid phase (Fig. 8).[25] This phase leads to very sharp He-diffraction peaks, characteristic for coherent Xe-domains about 800 A in size. As the Xe-coverage is increased above 0.33 the Xe-structure undergoes a transition from the commensurate $\sqrt{3}$ structure (C) to an incommensurate striped solid (SI) phase with superheavy walls (for details we refer the reader to Ref. 26). This weakly incommensurate solid is able to accommodate more Xe atoms than the commensurate phase by consisting of regions of commensurate domains separated by a regularly spaced array of striped denser domain walls. The domain walls have been found to be no sharp interfaces but relaxed broadened regions of increased density, 45 Xe-interrow distances wide (FWHM). Increasing coverage causes the commensurate domains to shrink and brings the walls closer together. The domain walls are thus a direct consequence of the system efforts to balance the competition between the lateral Xe-Xe and the Xe-Pt interactions. The C-SI transition can also be induced by decreasing the temperature below $\sim$ 60 K at constant coverage ($\theta_{Xe} \leq 0.33$); the driving force for this temperature induced CI-transition are anharmonic effects.[27]

The usual measure for the incommensurability of an I-phase is the misfit $m = (a_C - a_I)/a_C$ where a_C is the lattice parameter of the commensurate phase and a_I that of the incommensurate structure. For striped I-phases, the misfit has of course uniaxial character, being defined only along the direction perpendicular to the domain walls. Quantitative measurements[26] of the misfit during the C-SI transition of Xe on Pt(111) have revealed a power law of the form $m = 1/\ell \propto (1-T/T_c)^{0.51\pm0.04}$, i.e., the distance between nearest neighbor walls ℓ scales with the inverse square root of the reduced temperature. This square root dependence is the results of an entropy mediated repulsion between meandering nearest neighbor walls and is in accord with theoretical predictions.[28]

With increasing incommensurability the domain wall separation becomes progressively smaller until at a critical misfit of $\sim$ 6.5% the Xe domain wall lattice spontaneously rearranges from the striped to the hexagonal symmetry in a first order transition.[29] A further increase of the incommensurability by adding more and more Xe eventually results in an adlayer rotation to misalign itself with the substrate in order to minimize the increasing strain energy due to the defect concentration. This continuous transition starting at a rotated phase (HIR) follows a

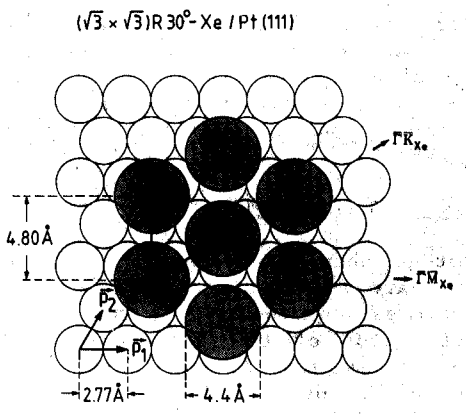

Fig. 8 Geometry of the commensurate ($\sqrt{3}$x$\sqrt{3}$) R30° Xe-monolayer on Pt(111).

power law $\phi \propto (m-0.072)^{1/2}$ starting at a critical separation between nearest neighbor walls $\ell_c \simeq 10$ Xe-interrow distances[29] (Fig. 9a).

Novaco and McTague[30] have shown that these adlayer rotations for monolayers far from commensurability are driven by the interconversion of longitudinal stress into transverse stress. These authors also showed that the rotational epitaxy involves mass density waves (MDW)[also known as static distortion waves (SDW)], i.e., there exists a periodic deviation of the position of monolayer atoms from their regular lattice sites. Indeed, it is the combination of rotation and small displacive distortions of the adatom net which allows the adlayer to minimize its total energy in the potential relief of the substrate. In a diffraction experiment, these mass density waves should give rise to satellite peaks.

Fuselier et al.[31] have introduced an alternative concept to explain the adlayer rotation: the "coincident site lattice". They pointed out that energetically more favorable orientations are obtained for rotated high-order commensurate structures. The larger the fraction of adatoms located in high-symmetry, energetically favorable sites, the larger the energy gain and the more effective the rotated layer is locked. It turns out that the predictions of the coincident site lattice concept for the rotation angle versus misfit agrees well with the Novaco-McTague predictions.

The experimental results do not allow so far to decide whether the Novaco-McTague mechanism involving MDW or the "coincident in lattice concept involving HOC structures, or may be both have the determining role in driving the adlayer rotation. In particular, no mass density wave satellites have been observed in electron and x-ray diffraction experiments from rotated monolayers[32] so far. In He diffraction scans of rotated Xe monolayers on Pt(111) we have, however, observed satellite peaks (see the peak marked by arrow, Fig. 2) at small Q-vectors. Originally we assigned these peaks to a higher-order commensurate superstructure[9]. However, Gordon[33] pointed out that these satellites could be due to the MDW. Here, we will show that both MDW as well as commensurate buckling satellites are present in the rotated Xe monolayers

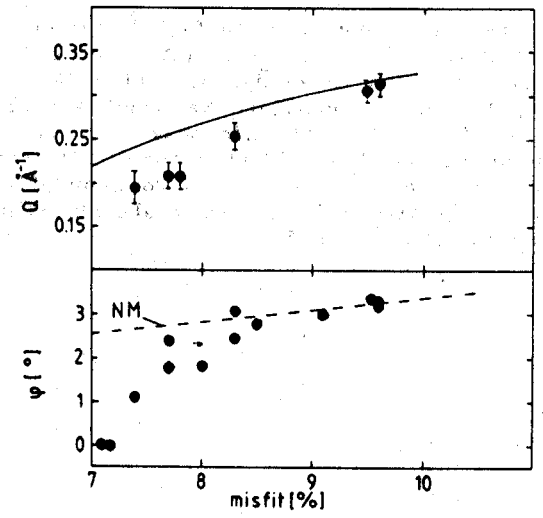

Fig. 9 Rotation angle ϕ of hexagonal incommensurate rotated Xe-monolayer on Pt(111) as a function of misfit m (bottom) and dispersion of the mass density wave satellites with m (top). The solid line is Gordon's relation (see text).

on Pt(111). The distinction between the two types of satellites is straightforward. As pointed out by Gordon, the wave vector, Q, of the MDW satellites should be subject to the following relation:

$$Q \simeq (8\pi/a_{Xe}^{R})\ m/\sqrt{3})\ (1+m/8)\ , \qquad (14)$$

with m the misfit, and a_{Xe}^{R} the lattice constant of the rotated Xe layer. For a not too large misfits, this MDW satellite should appear in the same direction as the principal reciprocal lattice vector of the Xe layer, i.e., in the $\bar{\Gamma}\ \bar{M}_{Xe}$ direction. On the other hand, according to its particular structure (Fig. 10b), the commensurate buckling should have its maximum amplitude in the $\bar{\Gamma}\ \bar{K}_{Xe}$ direction. Moreover, these commensurate buckling satellites should only be present at the particular coverages where a certain high-order commensurability becomes favorable, in the present case at monolayer completion (m = 9.6%) (see also Ref. 9), whereas the MDW satellites should be present in the entire misfit range where the Xe layer is rotated (7.2%-9.6%).

In Fig. 9b we show the dispersion of the MDW-satellites deduced from a series of diffraction scans like in Fig. 2, taken in the $\bar{\Gamma}\bar{M}_{Xe}$-direction, and compare them with Gordon's prediction for the MDW given above. The data follow qualitatively the predicted dependency; the agreement becomes quantitative at misfits $\geq$ 8%. The reason for the better agreement at large misfits is due to the fact that Gordon's analysis of the MDW (similar to Novaco-MacTague's model calculations) have been performed in the linear response approximation of the adsorbate-substrate interaction; this approximation is only justified at larger misfits, where the adlayer topography corresponds rather to a weakly modulated uniform layer than to a domain wall lattice.[34]

In Fig. 10(a) we show scans like in Fig. 2 but now measured in the $\bar{\Gamma}\,\bar{K}_{Xe}$ direction at small Q for rotated Xe layers of misfits 8% and 9.6%. At variance with the scans in the $\bar{\Gamma}\,\bar{M}_{Xe}$ direction (Fig. 2), a satellite peak is observed only for the complete Xe monolayer (m = 9.6%). Being present only at a particular misfit this peak does not originate from a MDW but from the buckling of a HOC-structure. The location of this satellite peak at Q = 0.28 $Å^{-1}$ corresponds to a buckling period of 23Å and can be ascribed to a high-order commensurate structure shown in Fig. 10(b) and described in detail in Ref. 9.

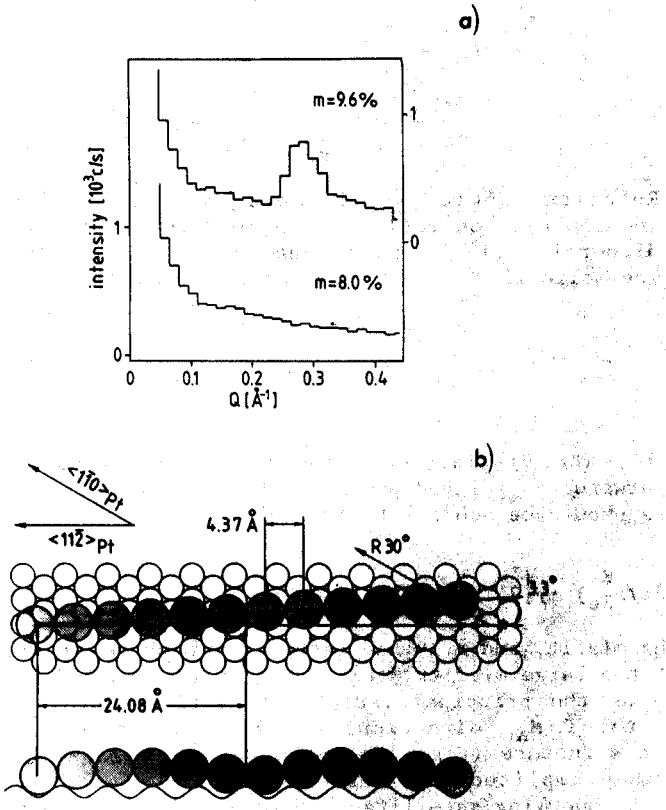

Fig. 10 a) Polar He-diffraction scan of rotated Xe monolayers on Pt(111) taken along the $\bar{\Gamma}\,\bar{K}_{Xe}$ azimuth at two misfits. b) Plane and side view of a 3.3° rotated Xe-domain at the misfit m = 9.6%.

MONOLAYER FILMS AND DYNAMICS OF COMPETING INTERACTIONS

When adsorbing a layer of atoms (for example rare gas atoms) on a substrate surface we are not dealing only with static interaction effects which determine the structure of the adlayer but also with dynamical interactions between collective excitations (for example phonons) of adlayer and substrate.

The phonon spectrum of a crystal surface consists of two parts: The bulk bands, which are due to the projection of bulk phonons onto the two-dimensional Brillouine zone of the particular surface, and the

specific surface phonon branches[8]. A surface phonon is defined as a localized vibrational excitation with an amplitude which has wavelike characteristics parallel to the surface and decays exponentially into the bulk, perpendicular to the surface. In Fig. 11a we display as an example the dispersion curves of the clean Pt(111) surface along the $\bar{\Gamma}\,\bar{M}_{Pt}$ azimuth[35]. The solid lines, termed S_1 and S_2, are specific surface phonon branches. These true surface modes only exist outside or in gaps of the projected bulk phonon bands of equivalent symmetry. The mode MS is an example of a 'surface resonance' which exists inside the bulk bands. Of particular interest is the lowest frequency mode S_1 below the transverse bulk band edge. In this mode, the atoms are preferentially vibrating in the plane defined by the surface normal and the propagation direction, i.e. in the sagittal plane. This wave is the famous Rayleigh wave.

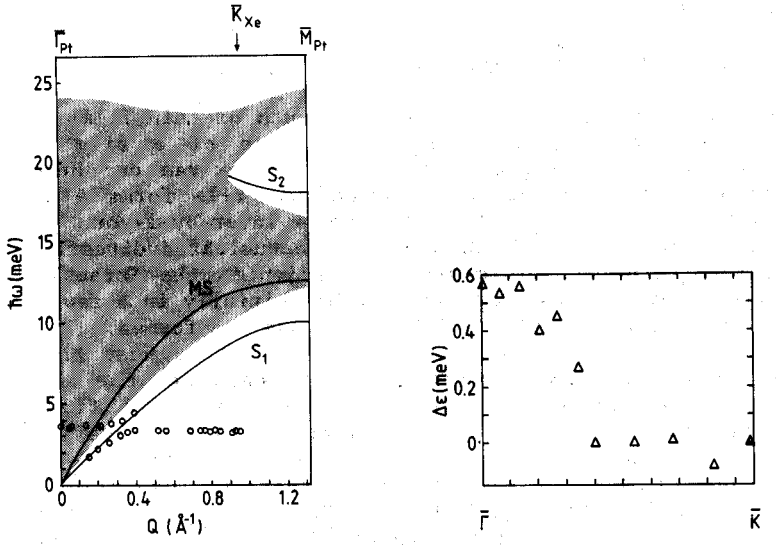

Fig. 11 Left: Surface phonon spectrum of the clean Pt(111) surface along the $\bar{\Gamma}\,\bar{M}_{Pt}$-azimuth (solid lines-discrete surface phonon branches, shaded regions-projected bulk bands) and of a Xe-monolayer adsorbed on this surface (dots). Right: Measured line width $\Delta\epsilon = [(\delta E)^2 - E_I^2]^{1/2}$, with δE the FWHM of the photon peak and E_I the intrinsic fundamental broadening (here $E_I = 0.32$ meV) of the Xe-monolayer phonon.

Adsorbing a layer of densely packed atoms on the substrate surface adds three additional phonon modes to the system; two in-plane modes and one mode with polarization perpendicular to the surface. The frequency and dispersion of these modes is governed by the "spring constants" which couple the adatoms laterally and to the substrate. In the following we concentrate on the perpendicular mode. In physisorbed systems, the electronic ground state of the adsorbate is only weakly perturbed upon adsorption. The physisorption potential is rather flat and shallow, i.e. the spring constant of the vertical adatom-motion is weak and the corresponding phonon frequencies are low (dots in Fig. 11a).

Being a dynamical system, the adlayer modes can couple to substrate phonon modes of the same polarization. The main effects of the phonon mediated coupling between adlayer and substrate, the mode hybridization

and life time shortening can be also seen in Fig. 11 for the system Xe/Pt(111).

At the Brillouin zone boundary the adlayer mode lying well below the substrate modes the influence of the substrate-adlayer coupling is negligible; neither dispersion nor linewidth of the adlayer mode are influenced by the substrate phonons. At the zone center in the whole region near Γ, however, where the adlayer mode overlaps the bulk phonon bands of the substrate a substantial linewidth-broadening, i.e. lifetime-shortening, is obvious (Fig. 11b). The excited adlayer modes decay by emitting phonons into the substrate; they become leaky modes. The most dramatic coupling effect, is a dramatic hybridization splitting around the crossing between the adlayer mode and the substrate Rayleigh wave obvious in Fig. 11a. A detailed quantitative account of these dynamical coupling effects has been given recently in Refs. 36 and 37.

MULTILAYER FILM GROWTH

1. Multilayer Growth Mode and Monolayer Structure

The mode of nucleation and initial growth of thin films is a matter of long standing interest. The growth-mode of a film is usually classified according to the morphology.[38] Frank-van der Merwe growth, type-1 growth: with increasing coverage the film forms a sequence of stable uniform layers, i.e. the film grows layer-by-layer. Volmer-Weber growth, type-3 growth: small 3D-cluster are nucleated directly on top of the bare substrate. An intermediate situation is the Stranski-Krastanov growth, type-2 growth: the deposit growths initially in a few (often only one) uniform layers on top of which 3D-islands are formed.

The important parameters which determine the equilibrium configuration of an heteroepitaxial system are the film-substrate interaction strength (not the corrugation as in the case of monolayer phases) and the lateral adatom-interaction in the film. Usual measures of these quantities are the isosteric heat of adsorption (which is identical to the quantity V_o defined in Eq. (11)) and the lateral adatom attraction e_1. Based on simple thermodynamics,[39] it was argued that uniform layer growth should be observed if the adsorbate-substrate interaction V_o is stronger than the lateral film interaction, e_1, i.e. for so called strong substrates. Weak substrates, on the other hand, should favor a three-dimensional cluster growth. Experiments designed to test these predictions[40] showed, however, that at low temperatures Frank-van der Merwe growth is restricted to a very narrow intermediate range of substrate strengths (see Fig. 12). Both, small as well as large V_o/e_1 values resulted in a nonuniform growth.

A more transparent and general criterion to analyze the type of growth to be expected results from the thermodynamic treatment given by Ernst Bauer many years ago.[41] The criterion for layer-by-layer (Frank van der Merwe) growth has been given recently by Bauer and van der Merwe in a more explicit form for an n-layer film:[42]

$$\gamma_{f(n)} + \gamma_{i(n)} - \gamma_s \leq 0 \ , \qquad (15)$$

with γ_s and $\gamma_{f(n)}$ the surface energies of the semi-infinte substrate and the n-monolayer film and $\gamma_{i(n)}$ the interfacial energy. Equation (15) is rigorously fulfilled in the trivial case of homoepitaxy, when $\gamma_{f(n)} = \gamma_s$ and $\gamma_{i(n)} = 0$. In the heteroepitaxial case the obvious condition is that $\gamma_f < \gamma_s$. The inequality has to be large enough to fulfill Eq. (15) because in general the interfacial energy has no reason to be negative

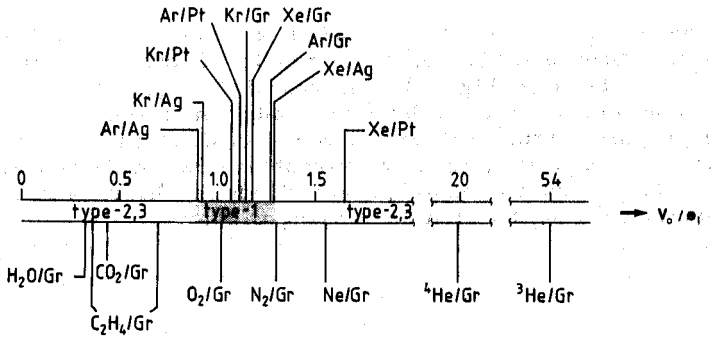

Fig. 12 Multilayer film growth modes of various adsorbate/substrate systems ordered on the scale of substrate strengths. Systems showing Frank-van der Merwe growth are marked by bars above the center line.

and, in addition, because substrate and film bulk have at least a different natural lattice constant and thus the first monolayer has in general an "unnatural" structure (at least an "unnatural" lattice constant); thus in general $\gamma_{f(1)} \geq \gamma_f$ and/or $\gamma_{i(1)}$ positive and non-negligible.

Bauer and van den Merwe[42] have included in $\gamma_{i(n)}$ the n-dependent strain energy of the film. In order to emphasize the role of the structure, Eq. (15) may be also written for each layer of the film as

$$\gamma_{f(n)} + \gamma_{i(n,n-1)} - \gamma_{f(n-1)} \leq 0 \ , \tag{16}$$

with $\gamma_{i(n,n-1)}$ the interfacial energy between the n-th layer and the (n-1)-layer film and thus e.g. for the second monolayer

$$\gamma_{f(2)} + \gamma_{i(2,1)} - \gamma_{f(1)} \leq 0 \ . \tag{17}$$

Because the surfaces of the n and n-1 film consist of the same atom species, $\gamma_{f(n)} \approx \gamma_{f(n-1)}$ with $\gamma_{f(n)}$ slightly smaller if the n-th layer has a more "natural" structure than the (n-1)th layer, which it certainly tends to have. However, if the structures of the two layers (n and n-1) differ, the interfacial energy $\gamma_{i(n,n-1)}$ becomes important and of course positive and Eq. (16) is not fulfilled. We may thus conclude that even if $\gamma_f < \gamma_s$ fulfilled, but the structure of the first monolayer differs appreciably from that of its own bulk, 3-D growth sets in above the first monolayer (Stranski-Krastanov mode). The set in of this mode may be retarded a few monolayers by long range influence of the substrate, but still there will be no layer-by-layer growth.

The rather restrictive condition for layer-by-layer growths that the structure (symmetry and lattice constant) of the first monolayer should be almost identical to that of the own bulk, explains also the reintrant non-wetting illustrated in Fig. 12. Indeed, on strong substrates the first adsorbed monolayer is in general compressed beyond the density of the close packed plane of its own bulk and thus no layer-by-lower growth takes place.

This behavior is consistent with a recent molecular dynamics simulation of Grabow and Gilmer,[44] the result of which is summarized in a 'phase' diagram shown in Fig. 13. The deposition on a fcc(100) substrate surface only occurs in a layer-by-layer mode for strong substrates $V_o/e_\ell \geq 1$ with negligible structural misfit $m \approx 0$ (thick line). The importance of the structural mismatch is also evident in the phase boundary between Stranski-Krastanov and Volmer-Weber growth which shifts substantially to larger substrate strengths with increasing misfit.

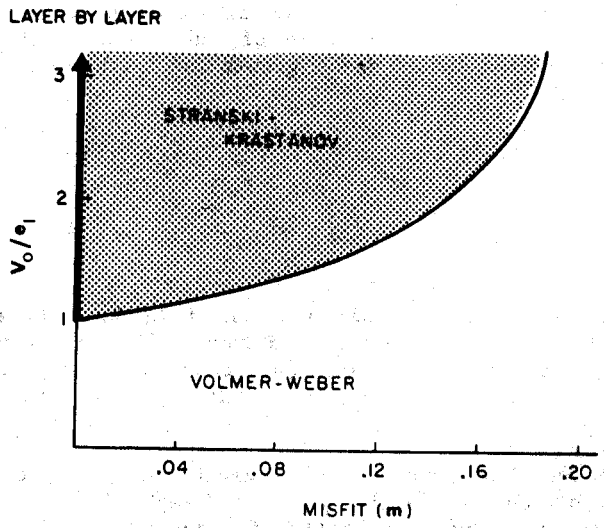

Fig. 13 "Phase" diagram of multilayer growth on a fcc(100) surface in the substrate strength V_o/e_ℓ-misfit plane, according to molecular dynamics calculations of Grabow and Gilmer.[44]

As will be shown below (section 5.2) the peculiar case of Xe/Pt(111), a strong substrate case growing yet layer-by-layer can be explained in the same frame. Indeed, the Xe monolayer is not compressed beyond its natural bulk lattice constant (4.34 Å at 25 K) simply because it becomes locked into a HOC-phase with exactly this lattice constant.

2. Epitaxial Multilayer Growth of Xe on Pt(111)

The He energy loss spectra shown in Fig. 3 contain besides lattice dynamics information also direct information concerning the growth characteristics of the Xe multilayers. This information is in the diffuse elastic peak, i.e., in the peak at zero energy exchange. This peak originates from scattering at defects and its intensity is a sensitive measure of surface disorder. From the comparison with spectra taken from surfaces of known disorder, we can infer that the monolayer is well ordered and the multilayers even better. For the 25 ML thick film in Fig. 3, the diffuse elastic peak has nearly vanished. This shows that the 25 ML film is very flat, and thus that Xe on Pt(111) exhibits complete wetting. This goes along with the layer-by-layer evolution of the surface phonon dispersion discussed in detail in Ref. 9 and 36.

The structure of the Xe multilayers has been characterized by measuring polar and azimuthal He-diffraction scans shown in Fig. 14. As already emphasized earlier at monolayer completion the Xe monolayer on 3.3°. Pt(111) is a Novaco-McTague rotated layer with rotation angle $\phi = \pm$ 3.3°. The azimuthal plots in Fig. 14 show that all consecutive layers growing on top of the first layer are likewise rotated by $\phi = \pm$ 3.3°. Lattice constant and average domain size, as deduced from the polar diffraction and average domain size, are also unchanged with increasing film thickness, i.e., $a_{Xe} = 4.33 \pm 0.03$ Å and average domain size ≈ 300 Å, respectively. Thus, the consecutive layers grow epitaxially on the preceding ones. Within experimental confidence there is no misfit between the nearest neighbor distances in the monolayer ($a_{Xe}^{R\text{-}ML} = 4.33$ Å, T = 25K) and in the bulk Xe ($a_{Xeb} = 4.34$ Å, T = 25 K). As already mentioned this structural compatibility, which leads to an unstrained layer-by-layer growth, appears to be a direct result of registry forces. Indeed Xe/Pt(111) being a "strong substrate" system, the monolayer lattice parameter would be expected, in the absence of registry forces,

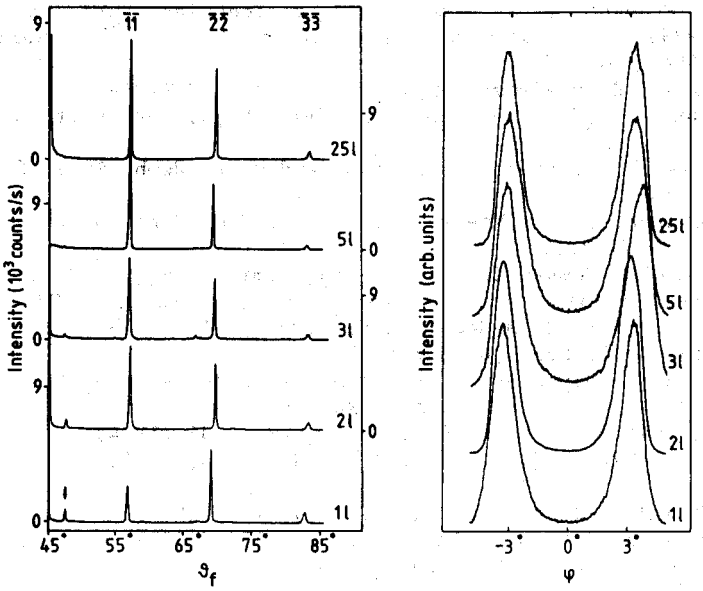

Fig. 14 Polar (left) and azimuthal (right) He diffraction scans of Xe-films of indicated thickness.

to be compressed well beyond the bulk value. However, as shown in chapter 3.2, at misfits of 9.6% the rotated monolayer locks into an energetically favorable high order commensurate structure. It is this high order commensurate locking of a fraction of adatoms which, by counterbalancing the tendency of the strong substrate to compress the monolayer lattice beyond the bulk value, allows for an unstrained layer-by-layer growth.

Note that the small peak at low Q-values in Fig. 14 is a MDW satellite already shown in Fig. 2. The very gradual disappearance of the mass density waves with increasing film thickness, emphasizes that the influence of the substrate on adsorbed multilayer films extends over several layers.

REFERENCES

1. M. Bienfait, Surf. Sci. 162, 411 (1985).
2. J. G. Dash, Physics Today, Dec. 1985, 26.
3. K. Kern, P. Zeppenfeld, R. David, and G. Comsa, J. Vac. Sci. Technol. A6, 639 (1988).
4. R. David, K. Kern, P. Zeppenfeld and G. Comsa, Rev. Sci. Instr. 57, 2771 (1986).
5. E. Zaremba and W. Kohn, Phys. Rev. B 15, 1769 (1977).
6. T. Engel and K. H. Rieder, Springer Tracts in Modern Physics (Springer, Berlin, 1982), Vol. 91.
7. P. Zeppenfeld, K. Kern, R. David and G. Comsa, Phys. Rev. Lett. 62, 63 (1989), A. M. Lahee, J. R. Manson and J. P. Toennies, Ch. Wöll, Phys. Rev. Lett. 57, 471 (1986).
8. K. Kern and G. Comsa, Adv. Chem. Phys., K. P. Lawley, ed. (Wiley, New York, 1989 p. 211).
9. K. D. Gibson and S. J. Sibener, Faraday Discuss. Chem. Soc. 80, 203 (1985); K. Kern, R. David, R. L. Palmer and G. Comsa, Phys. Rev. Lett. 56, 2823 (1986).
10. K. Kern, R. David and G. Comsa, Surf. Sci. 175, L669 (1986).
11. J. W. M. Frenken, B. J. Hinch and J. P. Toennies, Surf. Sci. 211/212, 21 (1989), A. C. Levi, R. Spadacini and G. E. Tommei, Surf. Sci. 182, 504 (1982).
12. G. Comsa and B. Poelsema, Appl. Phys. A38, 153 (1985).
13. B. Poelsema, L. K. Verheij and G. Comsa, Phys. Rev. Lett. 51, 2410 (1983)
14. J. Unguris, L. W. Bruch, E. R. Moog and M. B. Webb, Surf. Si. 109, 522 (1981).
15. J. P. McTague, J. Als Nielsen, J. Bohr and M. Nielsen, Phys. Rev. B25, 7765 (1982).
16. K. Kern and G. Comsa, in Physics and Chemistry of Solid Surfaces VII, R. Vanselow and R. F. Howe, eds. (Springer, Berlin, 1988) p. 64.
17. R. L. Park and H. H. Madden, Surf. Sci. 11, 188 (1968).
18. W. Steele, Surf. Sci. 36, 317 (1973).
19. D. Drakova, G. Doyen and F. V. Trentini, Phys. Rev. B32, 6399 (1985).
20. C. Girard and C. Girardet, Phys. Rev. B36, 909 (1987).
21. G. Vidali and M. W. Cole, Phys. Rev. B29, 6736 (1984).
22. K. Kern, R. David, P. Zeppenfeld and G. Gomsa, Surf. Sci. 195, 353 (1988).
23. J. Black and A. Janzen, Surf. Sci. 217, 199 (1989).
24. J. R. Chen and R. Gomer, Surf. Sci. 94, 456 (1980).
25. K. Kern, R. David, R. L. Palmer and G. Comsa, Phys. Rev. Lett. 56, 620 (1986).
26. K. Kern, R. David, P. Zeppenfeld, R. L. Palmer and G. Comsa, Solid State Comm. 62, 361 (1987).
27. M. B. Gordon and J. Villain, J. Phys. C18, 3919 (1985).
28. V. L. Pokrovsky and A. L. Talapov, Sov. Phys. JETP 51, 134 (1980).
29. K. Kern, Phys. Rev. B35, 8265 (1987).
30. A. D. Novaco and J. P. McTague, Phys. Rev. B19, 5299 (1979).
31. C. R. Fuselier, J. C. Raich and N. S. Gillis, Surf. Sci. 92, 667 (1980).
32. C. G. Shaw, S. C. Fain and M. D. Chinn, Phys. Rev. Lett. 41, 955 (1978), K. L. Damico et al., Phys. Rev. Lett. 53, 2250 (1984).
33. M. B. Gordon, Phys. Rev. Lett. 57, 2094 (1986).
34. H. Shiba, J. Phys. Soc. Jpn. 4R, 211 (1980).
35. K. Kern, R. David, R. L. Palmer, G. Comsa and T. S. Rahman, Phys. Rev. B33, 4334 (1986).
36. K. Kern, P. Zeppenfeld, R. David and G. Comsa, Phys. Rev. B35, 886 (1987), B. M. Hall, D. L. Mills, P. Zeppenfeld, K. Kern, U. Becher

and G. Comsa, Phys. Rev. B40, 6326 (1989).
37. B. M. Hall, D. L. Mills and J. Black, Phys. Rev. B32, 4932 (1985).
38. J. A. Venables, G. D. T. Spiller and M. Hanbücken, Rep. Prog. Phys. 47, 399 (1984).
39. D. E. Sullivan, Phys. Rev. B20, 3991 (1979).
40. M. Bienfait, J. L. Senguin, J. Suzanne, E. Lerner, J. Krim and J. G. Dash, Phys. Rev. B29, 983 (1984).
41. E. Bauer, Z. Kristallogr. 110, 372 (1958).
42. E. Bauer and J. H. Van der Merwe, Phys. Rev. B33, 3657 (1986).
43. R. J. Murihead, J. G. Dash and J. Krim, Phys. Rev. B29, 6985 (1984).
44. M. Grabow and G. H. Gilmer, Surf. Sci. 194, 333 (1988).